Modeling and Analysis of HetNets with mm-Wave Multi-RAT Small Cells Deployed Along Roads

Gourab Ghatak[†] [‡], Antonio De Domenico[†], and Marceau Coupechoux[‡]
[†]CEA, LETI, MINATEC, F-38054 Grenoble, France; [‡]LTCI, Telecom ParisTech, Université Paris Saclay, France.
Email: gourab.ghatak@cea.fr; antonio.de-domenico@cea.fr, and marceau.coupechoux@telecom-paristech.fr

***Abstract*—We characterize a multi tier network with classical macro cells, and multi radio access technology (RAT) small cells, which are able to operate in microwave and millimeter-wave (mm-wave) bands. The small cells are assumed to be deployed along roads modeled as a Poisson line process. This characterization is more realistic as compared to the classical Poisson point processes typically used in literature. In this context, we derive the association and RAT selection probabilities of the typical user under various system parameters such as the small cell deployment density and mm-wave antenna gain, and with varying street densities. Finally, we calculate the signal to interference plus noise ratio (SINR) coverage probability for the typical user considering a tractable dominant interference based model for mm-wave interference. Our analysis reveals the need of deploying more small cells per street in cities with more streets to maintain coverage, and highlights that mm-wave RAT in small cells can help to improve the SINR performance of the users.**

I. Introduction

To meet the tremendous increase in demand of high data rates in future wireless networks, the use of millimeter wave (mm-wave) bands is an attractive solution. However, mm-wave transmissions are associated with high path-loss and sensitivity to blockages [1]. Therefore, to maintain ubiquitous coverage, mm-wave technology will be overlayed on top of the existing classical μ-wave architecture. In an urban scenario, these mm-wave base stations can be deployed along the roads e.g. on top of buildings and lamp-posts to cater to the needs of outdoor users.

In the context of heterogeneous networks, the user performance is often analyzed with the help of stochastic geometry, i.e., in terms of signal to interference plus noise (SINR) coverage probability and rate coverage probability [2]. These metrics have been derived to investigate single-tier [3] and multi-tier mm-wave networks [4]. Elshaer et al. [5] have analyzed a multi-tier network with μ-wave macro cells and mm-wave small cells in terms of user association, SINR and rate coverage, in both uplink and downlink scenarios. However, in these works, the base station locations are modeled as classical homogeneous Poisson point processes on the $\mathbb{R}^2$ plane [6], or as Poisson cluster processes [7], which are not realistic representations of the network architecture in an urban scenario.

To address this issue, we investigate a network geometry, where the small cells are deployed along the roads. In this regard, we take help of a framework introduced by Morlot [8] based on a Poisson line tessellation to model the roads in an urban scenario. Furthermore, we consider that the small cells are equipped with multi-radio access technology (RAT), thereby enabling them to opportunistically serve the users with both micro- and mm-wave bands.

The contribution of this paper is summarized as follows. We characterize a novel multi-tier network with small cells deployed along the streets, and derive the association probabilities of the typical user. Then, we consider a dominant interferer based model to characterize the mm-wave interference. On one hand, this approach of modeling mm-wave interference is more tractable than to consider all interfering base stations, whereas on the other hand, we show that it is more accurate in characterizing the SINR coverage as compared to a noise-limited approach [9]. Using these results, we derive the SINR coverage probability of the typical user, and investigate the effect of different deployment parameters of the network on the SINR performance. Our analysis reveals the fact that in cities with more streets, the operator must necessarily deploy more small cells per street to maintain the SINR coverage. Moreover, we highlight that the utility of multi-RAT base stations is not only limited to providing high data rate access to the users, but also that this technology, by taking advantage of the directional antennas, can considerably improve the SINR. Finally, we show that this gain in SINR performance brought by mm-wave, reaches a maximum value for a certain small cell deployment density, depending on the street density, and saturates at denser deployments.

The rest of the paper is organized as follows: in Section II we introduce the network architecture. We derive some preliminary results related to the mm-wave interference model, and the network geometry, in Section III. In Section IV and V we compute the association probabilities and SINR coverage probability of a typical user, respectively. In Section VI-A we present some numerical results to discuss salient trends of the network. Finally, the paper concludes in Section VII.

II. System Model

We consider a multi-tier cellular network consisting of macro base stations (MBSs) and small cell base stations (SBSs). The MBSs are deployed to ensure continuous coverage to the users. Whereas, the multi-RAT SBSs, deployed along the roads, locally provide high data rate by jointly exploiting μ-wave and mm-wave bands. We assume that the same μ-wave band is shared by MBSs and SBSs. From the

The research leading to these results are jointly funded by the European Commission (EC) H2020 and the Ministry of Internal affairs and Communications (MIC) in Japan under grant agreements N^{o} 723171 5G MiEdge.

perspective of the users, the base stations can either be in line-of-sight (LOS), or non line-of-sight (NLOS). In our analysis, we use the subscript notation t, v, r to characterize the base stations, where $t \in \{M, S\}$ denotes the tier (MBS or SBS), $v \in \{L, N\}$ denotes the visibility state (LOS or NLOS), and $r \in \{\mu, m\}$ denotes the RAT (μ-wave or mm-wave).

A. Network Model

The MBS locations are modeled as a homogeneous Poisson point process (PPP) ϕ_M with intensity λ_M. On the contrary, the roads are modeled as Poisson line processes (PLP) with intensity λ_R. The SBSs are deployed on the PLP tessellation of the roads, according to a PPP ϕ_S with intensity λ_S. We denote by ϕ_i, the 1D PPP on each road, where i is the index of the roads. Furthermore, we consider outdoor users, which are modeled as stationary PPP ϕ_{OU} along the roads, with an intensity λ_{OU}. Thus, both the SBSs and users are modeled by a Cox process driven by the intensity measure of the road process [10]. In the following, we carry out our analysis from the perspective of the typical user, located at the origin.

B. Blockage and Path-loss

We assume a LOS ball model to categorize the MBSs into either LOS or NLOS processes, from the perspective of a user: ϕ_{ML} and ϕ_{MN}, respectively. As per the LOS ball approximation introduced in [3], let D_M be the MBS LOS ball radius. The probability of the typical user to be in LOS from a MBS at a distance r is $p_M(r) = 1$, if $r < D_M$, and $p_M(r) = 0$, otherwise. All the SBSs lying on the same road as that of the typical user are considered to be in LOS, denoted by the process ϕ_{SL}. All the other SBSs, are considered to be in NLOS, denoted by the process ϕ_{SN}.

We assume that the path-loss at a distance d_{tvr} from a transmitter is given by: $l_{tvr}(d) = K_{tvr} d_{tvr}^{-\alpha_{tvr}}$. K and α are the path-loss coefficient and exponent, respectively. For μ-wave communications, we assume a fast fading that is Rayleigh distributed with variance equal to one. On the contrary, due to the low local scattering in mm-wave [1], we consider a Nakagami fading for mm-wave communications [9]. Moreover let G_0 be the directional antenna gain in mm-wave transmissions. Thus, the average received power is given by $P_{tvr} = P_t K_{tvr} d_{tvr}^{-\alpha_{tvr}}$, in μ-wave and $P_{tvr} = G_0 P_t K_{tvr} d_{tvr}^{-\alpha_{tvr}}$ in mm-wave; where P_t is the transmit power of a BS of tier t.

III. Preliminaries

A. Interference in LOS SBS mm-Wave Operation

We assume that in mm-wave operations, a user experiences interference only from the neighboring mm-wave SBS, due to the highly directional antenna. In Section VI-A, we prove the accuracy of this assumption with Monte Carlo simulations. In this section, we model the probability that the typical user experiences interference from the neighboring SBS.

Definition 1. *We define 'spillover' as the region of interference generated by a mm-wave SBS to the coverage area of a neighboring SBS, while serving a user near its cell edge.*

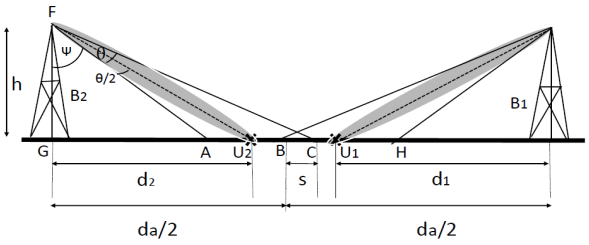

Figure 1: Interference in mm-wave operation.

Lemma 1. *For a typical user being served with mm-wave, the probability of experiencing mm-wave interference (p_G) from its closest neighboring SBS is given by* (1) *on top of the next page, where θ is the beam-width of the directional antenna,* $d' = h \tan\left(\tan^{-1}\frac{x}{2h} - \frac{\theta}{2}\right)$, $d^* = \max\left(\frac{h-\sqrt{h^2-8h^2\tan\left(\frac{\theta}{2}\right)}}{2\tan\left(\frac{\theta}{2}\right)}, 2h\tan\left(\frac{\theta}{2}\right)\right)$, $\hat{d} = \frac{h+\sqrt{h^2-8h^2\tan\left(\frac{\theta}{2}\right)}}{2\tan\left(\frac{\theta}{2}\right)}$ *and* $f_{xy}(x,y) = 2\lambda_S^2 \exp(-\lambda_S(x))$.

Proof. Let the typical user U_1 (see Fig. 1) be located at a distance d_1 from its serving SBS B_1. U_1 experiences mm-wave interference from the neighboring BS B_2 if it lies in the spillover region, s of B_2. The probability of this event is calculated as: $\mathbb{P}\left(d_1 \geq \frac{d_a}{2} - s\right) = \exp\left(-\lambda_S\left(\frac{d_a}{2} - s\right)\right)$, where d_a is the inter SBS distance. Now, B_2 produces spillover to the coverage area of B_1, if the distance of the user U_2 from B_2 is greater than some distance d', and as a result, the extremest point of its serving antenna beam crosses the cell boundary. Thus, B_2 produces spillover in the coverage area of B_1, if the user U_2 lies in the region $d' \leq d_2 \leq \frac{d_a}{2}$. The probability that at least one such user exists, is given by $1-\exp\left(\mu_{OU}\left(\frac{d_a}{2} - d'\right)\right)$. Now, the spillover s to the coverage area of B_1 can be calculated as:

$$s = GC - \frac{d_a}{2} = h\tan(\theta + \psi) - \frac{d_a}{2}$$
$$= h\tan\left(\frac{\theta}{2} + \tan^{-1}\frac{d_2}{h}\right) - \frac{d_a}{2}, \quad (2)$$

where ψ is the angle of depression from the top of B_2 to the nearest point of the serving beam on the ground. Now, d' is obtained from the condition $s > 0$, i.e., d' is the minimum distance of U_2 from B_2, beyond which positive spillover occurs. Finally, d^* and $\hat{d}$ are obtained from the conditions $d' \geq 0$ and $s \leq \frac{d_a}{2}$. These conditions state, respectively, that B_2 does not cause spillover to B_1 while serving any U_2 located on the left side of B_2, and that the spillover s is limited to the left side of B_1. Now, substituting the value of s, writing $d_2 = d_a - d_1$, and taking the expectation with respect to d_a (denoted by X) and d_1 (denoted by Y), i.e., $f_{XY}(x,y) = 2\lambda_S^2 \exp(-\lambda_S(x))$, completes the proof. See [11] for a detailed proof. □

B. Characterization of the NLOS SBS Cox Process

Lemma 2. *The pdf of the distance from a typical user to the nearest NLOS SBS is given by* (3) *on top of the next page.*

$$p_G = \int_{d^*}^{\hat{d}} \int_{d'}^{\frac{\pi}{2}} \exp\left(-\mu_S\left(x - h\tan\left(\frac{\theta}{2} + \tan^{-1}\frac{y}{h}\right)\right)\right)\left(1 - \exp\left(\mu_{OU}\left(\frac{x}{2} - d'\right)\right)\right) f_{yx}(y,x)dydx \tag{1}$$

$$f_{d_{S1}}(x) = 2\pi\lambda_R \exp\left(-2\pi\lambda_R\left(x + \int_0^x \exp\left(-2\lambda_S\sqrt{x^2 - r^2}\right)dr\right)\right)\left[2\lambda_S x \int_0^x \frac{\exp(-2\lambda_S\sqrt{x^2 - r^2})}{\sqrt{x^2 - r^2}}dr\right] \tag{3}$$

Proof. Consider that the nearest point of the NLOS SBS process from the typical user is at a distance x. Accordingly, the ball $\mathcal{B}(o,x)$ does not contain any NLOS SBS. We know that the number of lines of the Poisson line process hitting $\mathcal{B}(0,x)$ is Poisson distributed with parameter $2\pi\lambda_R x$ [10]. Now, a randomly orientated line at a distance r from the origin, has a chord length of $2\sqrt{x^2 - r^2}$, and a void probability $\exp(-2\lambda_S\sqrt{x^2 - r^2})$, in the circle $\mathcal{B}(0,x)$. As a result, the probability of no points falling in this ball, averaged over the number of lines, is calculated as:

$$\begin{aligned} F_{d_{S1}}(x) &= \sum_{n=0}^{\infty} \frac{(2\pi\lambda_R x)^n \exp(-2\pi\lambda_R x)}{n!\,(x^n)} \\ &\left[\int_{r_1,r_2,\ldots,r_n=0}^{x} \prod_{i=1}^{n} \exp\left(-2\lambda_S\sqrt{x^2 - r_i^2}\right)dr_i\right] \\ &= \sum_{n=0}^{\infty} \frac{(2\pi\lambda_R x)^n \exp(-2\pi\lambda_R x)}{n!\,(x^n)} A_2^n, \end{aligned}$$

where $A_2 = \int_0^x \exp\left(-2\lambda_S\sqrt{x^2 - r^2}\right)dr$ is from the symmetry of the process ϕ_S. The term x^n in the denominator, appears as a result of the Palm expectation of the distance of each of these lines. Finally, the PDF of the distance x is calculated by differentiating $F_{d_{S1}}(x)$. See [11] for a detailed derivation. □

Lemma 3. *([8], Theorem III.1). The SBS process ϕ_S is stationary and isotropic, with intensity $\pi\lambda_R\lambda_S$. Under Palm, it is the sum of ϕ_S, of an independent Poisson point process on a line through the origin O with a uniform independent angle, and of an atom at O.*

Lemma 4. *The probability generating functional (PGF), for a class of radially symmetric functions ν, of the Poisson Line Cox Process ϕ_S is given by* (4) *on top of the next page.*

Proof. The proof is similar to that of Theorem III.2 in [8]. See [11] for the derivation. □

Lemma 5. *The PGF for a class of radially symmetric functions ν, of a PPP on a randomly oriented line, passing through a point at a distance d from the origin, is given by* (5) *on top of the next page.*

Proof. Without loss of generality, we assume that the line passes through $(d,0)$ inclined at an angle θ with the x-axis. Thus a point on the line at a distance t from $(d,0)$ is at a distance $r = \sqrt{(d + t\cos\theta)^2 + (t\sin\theta)^2}$, from the origin. Taking the PGF along all such points completes the proof. □

IV. Association Probabilities

We assume that the BSs send their control signals in the μ-wave band, due to the higher reliability of μ-wave signals as compared to the mm-wave signals [12]. For the association, a user compares the μ-wave signals from the strongest LOS and NLOS SBS and MBS. According to our MBS LOS ball assumption, the received power from and LOS MBS is always greater than that received from and NLOS MBS. Accordingly, for association, we consider an NLOS MBS if and only if an LOS MBS is absent. In case the user is associated with an MBS or an NLOS SBS, it is served in the μ-wave band. Whereas, in case it is associated to an LOS SBS, the user compares the power received in the μ-wave and mm-wave band, and selects the RAT providing the highest power.

A. Tier Selection Probabilities

In the following analysis, we drop the subscript μ for ease of notation. The term '1' in the subscript refers to the strongest BS of type tv. Accordingly, d_{tv1} denotes the distance corresponding to the strongest base station of tier tv. Let the pdf of d_{tv1} be denoted by $f_{tv1}(x)$. For, $\{t,v\} = \{SN\}$, $f_{tv1}(x)$ is given by (3). Whereas, for $\{t,v\} \neq \{SN\}$, the expressions for f_{tv1}, can easily be obtained by differentiating the void probabilities of the corresponding processes [10] :

$$\begin{aligned} f_{SL1}(x) &= 2\lambda_S \exp(-2\lambda_S x) \\ f_{ML1}(x) &= 2\pi\lambda_M x \exp\left(-\pi\lambda_M x^2\right); \quad x < D_M \\ f_{MN1}(x) &= 2\pi\lambda_M x \exp\left(-\pi\lambda_M\left(x^2 - D_M^2\right)\right); \; x \geq D_M \end{aligned}$$

Lemma 6. *The tier selection probability of a user with a LOS and NLOS MBS and LOS SBS is given by* (6) *on top of the next page, where,*

$$\begin{aligned} W_{ML} &= 1 - \exp\left(-\pi\lambda_M\left(\frac{P_S}{P_M}\right)^{-\frac{2}{\alpha_{ML}}} x^{\frac{2\alpha_{SL_\mu}}{\alpha_{ML}}}\right), \\ W_{MN} &= 1 - \exp\left(-\pi\lambda_M\left(\frac{P_S}{P_M}\right)^{-\frac{2}{\alpha_{MN}}} x^{\frac{2\alpha_{SL_\mu}}{\alpha_{MN}}}\right), \\ W_1 &= \mathbb{E}[\mathbb{1}(ML)] = 1 - \exp(-\pi\lambda_M D_M^2), \\ W_2 &= \mathbb{E}_{d_{SN1}}\left[1 - \exp\left(-2\mu d_{SN1}^{\frac{\alpha_{SN_\mu}}{\alpha_{SL_\mu}}}\right)\right]. \end{aligned}$$

Here, $\mathbb{1}(.)$ is the indicator function, and accordingly, $\mathbb{E}[\mathbb{1}(ML)]$ denotes the probability that at least one LOS MBS exists.

$$G_{\phi_S}(\nu) = \exp\left(-2\pi\lambda_R\left(\int_0^\infty 1-\exp\left(-2\lambda_S\int_0^\infty 1-\nu\left(\sqrt{r^2+t^2}\right)dt\right)\right)dr\right) \tag{4}$$

$$G_{\phi_i,d}(\nu) = \frac{1}{2\pi}\int_0^{2\pi}\exp\left(-2\lambda_S\int_0^\infty\left(1-\nu\left(\left(d^2+t^2+2td\cos\theta\right)^{\frac{1}{2}}\right)\right)dt\right)d\theta \tag{5}$$

$$\begin{aligned}
\mathbb{P}_{ML} &= 2\lambda_S W_1 \mathbb{E}_{d_{SN1}}\left[1-\exp\left(-\pi\lambda_M\left(\frac{P_S}{P_M}\right)\right)^{-\frac{2}{\alpha_{ML}}} d_{S1}^{\frac{2\alpha_{SN\mu}}{\alpha_{ML}}}\right]\int_0^\infty\left(W_{ML}\exp(-2\lambda_S x)\right)dx,\\
\mathbb{P}_{MN} &= 2\lambda_S(1-W_1)\mathbb{E}_{d_{SN1}}\left[1-\exp\left(-\pi\lambda_M\left(\frac{P_S}{P_M}\right)\right)^{-\frac{2}{\alpha_{MN}}} d_{S1}^{\frac{2\alpha_{SN\mu}}{\alpha_{MN}}}\right]\int_0^\infty\left(W_{MN}\exp(-2\lambda_S x)\right)dx,\\
\mathbb{P}_{SL} &= 2\lambda_S W_2\left(W_1\int_0^\infty(1-W_{ML})\exp(-2\lambda_S x)dx+\left(\int_0^\infty(1-W_{MN})\exp(-2\lambda_S x)dx\right)(1-W_1)\right)
\end{aligned} \tag{6}$$

Proof. The probability of association with a LOS and NLOS MBS are given by:

$$\begin{aligned}
\mathbb{P}_{ML} &= \mathbb{E}[\mathbb{1}(ML)]\mathbb{P}(P_{ML1}\geq P_{SL1})\mathbb{P}(P_{ML1}\geq P_{SN1})\\
\mathbb{P}_{MN} &= \left(1-\mathbb{E}[\mathbb{1}(ML)]\right)\mathbb{P}(P_{MN1}\geq P_{SL1})\\
&\quad\ \mathbb{P}(P_{MN1}\geq P_{SN1}).
\end{aligned}$$

The terms in the above equation for $\mathbb{P}_{MN}$ are calculated as:

$$\begin{aligned}
&\mathbb{P}(P_{MN1}\geq P_{SL1})\\
&=\mathbb{P}\left(K_\mu P_M d_{MN1}^{-\alpha_{MN}}\geq K_\mu P_S d_{SL1}^{-\alpha_{SL}}\right)\\
&=\mathbb{P}\left(d_{MN1}\leq\left(\frac{P_S}{P_M}\right)^{-\frac{1}{\alpha_{MN}}} d_{SL1}^{\frac{\alpha_{MN}}{\alpha_{SL}}}\right)\\
&=\mathbb{E}_{d_{SL1}}\left[1-\exp\left(-\pi\lambda_M\left(\frac{P_S}{P_M}\right)^{-\frac{2}{\alpha_{MN}}} d_{SL1}^{\frac{2\alpha_{SN\mu}}{\alpha_{MN}}}\right)\right].
\end{aligned}$$

Similarly, we can obtain $\mathbb{P}(P_{ML1}>P_{SL1})$, $\mathbb{P}(P_{MN1}\geq P_{SN1})$, and $\mathbb{P}(P_{ML1}\geq P_{SN1})$. Now,

$$\begin{aligned}
\mathbb{P}_{SL} = \mathbb{P}(P_{SL1}>P_{SN1})\big(&\mathbb{P}(P_{SL1}>P_{ML1})\mathbb{E}[\mathbb{1}(ML)]\\
&+\mathbb{P}(P_{SL1}>P_{MN1})\left(1-\mathbb{E}[\mathbb{1}(ML)]\right)\big).
\end{aligned}$$

$$\mathbb{P}(P_{SL1}>P_{SN1}) = \mathbb{E}_{d_{SN1}}\left[1-\exp\left(-2\mu d_{SN1}^{\frac{\alpha_{SN\mu}}{\alpha_{SL\mu}}}\right)\right]$$

is calculated using the void probability of the LOS SBS process, and $\mathbb{P}(P_{SL1}>P_{Mv1}) = 1-\mathbb{P}(P_{Mv1}>P_{SL1})$, for $v\in\{L,M\}$. The association probability with the NLOS SBS tier can be calculated as: $\mathbb{P}_{SN} = 1-\mathbb{P}_{ML}-\mathbb{P}_{MN}-\mathbb{P}_{SL}$. □

Lemma 7. *Given that a user is associated to a tier t of visibility state v, the probability density function (pdf) of the distance of the serving BS is given by:*

$$\hat{f}_{tv1}(x) = \frac{f_{tv1}(x)}{\mathbb{P}_{tv}}\prod_{\forall(t'v'\neq tv)}\mathbb{P}(\phi_{t'v'}\cap(0,x)=0), \tag{7}$$

B. RAT Selection Probability

In case of LOS SBS association, the user selects μ-wave or mm-wave RAT by comparing the received power from the selected SBS in these two bands.

Lemma 8. *The conditional mm-wave selection probability, given that it is associated with an LOS SBS is given by:*

$$\mathbb{P}_m = \exp\left(-2\lambda_S\left(\frac{K_\mu}{K_m G_0}\right)^{\frac{1}{\alpha_{SL\mu}-\alpha_{SLm}}}\right)$$

Proof. We have :

$$\begin{aligned}
\mathbb{P}_m &= \mathbb{P}(r=mm|t=SL)\\
&= \mathbb{P}(K_m G_0 P_S d_{SL1}^{-\alpha_{SLm}} > K_\mu P_S d_{SL1}^{-\alpha_{SL\mu}})\\
&= \mathbb{P}\left(d_{SL}>\left(\frac{K_\mu}{K_m G_0}\right)^{\frac{1}{\alpha_{SL\mu}-\alpha_{SLm}}}\right).
\end{aligned}$$

Taking the void probability completes the proof. □

The overall association probability of the typical user is given by $\mathbb{P}_{tvr} = \mathbb{P}_{tv}\mathbb{P}_m$ where, the term $\mathbb{P}_m$ is considered only in case of association with a base station of type SL. In case of other tiers, we have exclusively, $r=\mu$.

V. SINR Coverage Probabilities

According to the derived association probabilities, the SINR coverage probability is obtained as:

Theorem 1. *The conditional SINR coverage probability, given that the typical user is associated to a BS to type 'tv' in μ-wave and mm-wave are given by* (8) *and* (9)*, respectively, where, the expectations with respect to the serving BS distance d_{tv1} is taken as per Lemma 7. G_ϕ and G_ϕ^y refer to the PGF w.r.t. the process ϕ, and the PGF w.r.t. ϕ taken according to the reduced Palm distribution with the first point at y, respectively.*

$$\mathbb{P}\left(SINR_{tv\mu} \geq \gamma\right) = \begin{cases} \mathbb{E}\left[\exp\left(-\frac{\gamma\sigma_\mu^2}{P_S K_\mu d_{tv1}^{-\alpha_{SL\mu}}}\right)\right] \cdot \prod\limits_{\substack{\{t'v'\} \\ \neq\{tv\}}} \mathbb{E}_{d_{tv1}}\left[G_{\phi_{t'v'}}\left(\frac{P_t||x||^{\alpha_{t'v'}}}{P_t||x||^{\alpha_{t'v'}}+\gamma P_t' d_{tv1}^{\alpha_{tv}}}\right)\right] \cdot \\ \cdot \mathbb{E}_{d_{tv1}}\left[G_{\phi_{tv}}^{tv1}\left(\frac{||x||^{\alpha_{tv}}}{||x||^{\alpha_{tv}}+\gamma d_{tv1}^{\alpha_{tv}}}\right)\right]; \qquad \forall\{tv\} \neq \{SN\} \\ \mathbb{E}\left[\exp\left(-\frac{\gamma\sigma_\mu^2}{P_S K_\mu d_{SN1}^{-\alpha_{SL\mu}}}\right)\right] \cdot \prod\limits_{\substack{\{t'v'\} \\ \neq\{SN\}}} \mathbb{E}_{d_{SN1}}\left[G_{\phi_{t'v'}}\left(\frac{P_S||x||^{\alpha_{t'v'}}}{P_S||x||^{\alpha_{t'v'}}+\gamma P_t' d_{SN1}^{\alpha_{SN}}}\right)\right] \cdot \\ \cdot \mathbb{E}_{d_{SN1}}\left[G_{\phi_{SN}}^{SN1}\left(\frac{||x||^{\alpha_{SN}}}{||x||^{\alpha_{SN}}+\gamma d_{SN1}^{\alpha_{SN}}}\right)\right] \cdot \mathbb{E}_{d_{SN1}}\left[G_{\phi_i, d_{SN1}}^{SN1}\left(\frac{||x||^{\alpha_{SN}}}{||x||^{\alpha_{SN}}+\gamma d_{SN1}^{\alpha_{SN}}}\right)\right]; \quad \text{otherwise.} \end{cases} \tag{8}$$

$$\mathbb{P}\left(SINR_{SLm} \geq \gamma\right) = \sum_{n=1}^{n_0} (-1)^{n+1} \binom{n_0}{n} \mathbb{E}_{d_{SL1}}\left[\exp\left(-\frac{n\gamma\sigma_{mm}^2}{K_m P_S d_{SL1}^{-\alpha_{SLm}} G_0}\right)\right] \mathbb{E}\left[\left(\frac{d_{SL2}^{\alpha_{SLm}}}{d_{SL2}^{\alpha_{SLm}} + \gamma p_G d_{SL1}^{\alpha_{SLm}}}\right)\right] \tag{9}$$

Proof. We present the proof sketch for one association case. The other cases follow on similar lines. In case the user is associated to a NLOS SBS, we have:

$$SINR_{SN\mu} = \frac{P_S K_\mu h_{SN1} d_{SN1}^{-\alpha_{SN}}}{\sigma_\mu^2 + I_{SN} + I_{ML} + I_{SL} + I_{MN}}$$

$$\begin{aligned} &\mathbb{P}\left(SINR_{SN\mu} \geq \gamma\right) \\ &= \mathbb{P}\left(h_{SN1} > \frac{\gamma\left(\sigma_\mu^2 + I_{SN} + I_{ML} + I_{SL} + I_{MN}\right)}{P_S K_\mu d_{SN1}^{-\alpha_{SN\mu}}}\right) \end{aligned}$$

where, $I_{(.)}$ are the interference terms from different tiers. The expression is evaluated by using the tail distribution of the exponentially distributed h_{SN1}, followed by the independence of the different BS process. We provide the steps for evaluation of the term corresponding to the MBS LOS process. The other terms are obtained similarly.

$$\begin{aligned} &\mathbb{E}\left[\exp\left(-\frac{\gamma \sum\limits_{\phi_{ML}} I_{ML}}{P_S K_\mu d_{SN1}^{-\alpha_{SN\mu}}}\right)\right] \\ &= \mathbb{E}\left[\exp\left(-\frac{\gamma P_M K_\mu \sum\limits_{\phi_{ML}} h_{MLi} d_{MLi}^{-\alpha_{ML}}}{P_S K_\mu d_{SN1}^{-\alpha_{SN\mu}}}\right)\right] \\ &\overset{a}{=} \mathbb{E}\left[\prod_{\phi_{ML}} \exp\left(-\frac{\gamma P_M h_{MLi} d_{MLi}^{-\alpha_{ML}}}{P_S d_{SN1}^{-\alpha_{SN\mu}}}\right)\right] \\ &\overset{b}{=} \mathbb{E}\left[\prod_{\phi_{ML}} \frac{P_S d_{MLi}^{\alpha_{ML}}}{P_S d_{ML}^{\alpha_{ML}} + \gamma P_M d_{SN1}^{\alpha_{SN}}}\right] \\ &= \mathbb{E}_{d_{SN1}}\left[G_{\phi_{ML}}\left(\frac{P_S x^{\alpha_{ML}}}{P_S x^{\alpha_{ML}} + \gamma P_M d_{SN1}^{\alpha_{SN}}}\right)\right], \end{aligned}$$

The step (a) follows from the independence of the variables h_{MLi}, (b) is obtained by applying the Laplace functional of h_{MLi}. Moreover, as per Lemma 3, in case the user is associated to an NLOS SBS, the interfering NLOS SBS process ϕ_{SN} consists of the stationary process ϕ_S and a line process ϕ_i, passing though the serving SBS. Accordingly, the SINR coverage probability for NLOS SBS association has an additional term, which takes the line process into account. Furthermore, for the mm-wave association case, we have:

$$\begin{aligned} &\mathbb{P}\left(SINR_{SLm} \geq \gamma\right) = \\ &\mathbb{P}\left(h_{SL1} \geq \frac{\gamma\sigma_{mm}^2 + \gamma K_m P_S h_{SL2} d_{SL2}^{-\alpha_{SLm}} p_G G_0}{K_m P_S d_{SL1}^{-\alpha_{SLm}} G_0}\right), \end{aligned}$$

where d_{SL2} is the distance of the neighboring SBS. Using Alzer's lemma for the tail distribution of a gamma random variable with integer parameter [13], Lemma 1, and from the definition of the PGF, the result (9) follows. Note that in (9), we take the expectation with respect to the joint distribution of d_{SL1} (denoted by x) and d_{SL2} (denoted by y): $f_{X,Y}(x.y) = 2\lambda_S^2 \exp(-\lambda_S(x+y))$. See [11] for the derivation of $f_{X,Y}(x.y)$. □

Finally, the overall coverage probability is calculated as:

$$\mathbb{P}_C(\gamma) = \sum_{t\in\{M,S\},\, v\in\{L,N\},\, r\in\{\mu,m\}} \mathbb{P}(SINR_{t,v,r} > \gamma | t, v, r) \mathbb{P}_{tvr},$$

where $r = m$ is considered only in case of $\{tv\} = \{SL\}$.

VI. Numerical Results and Discussion

In this section, we provide some numerical results to discuss the salient trends of the network. We assume transmit powers of $P_M = 45$ dBm and $P_S = 30$ dBm. Parameters K_{tvr} are derived as $K_{tvr} = \left(\frac{c}{4f_r\pi}\right)^2$, where f_r is the carrier frequency of RAT r [5]. We consider carrier frequencies of 60 GHz for mm-wave and 2.3 GHz for μ-wave. The path-loss exponents are assumed to be $\alpha_{tNr} = 4$ and $\alpha_{tLr} = 2$ for the NLOS and LOS base stations. The Nakagami fading parameter n_0 is taken to be 3 [3]. Furthermore, we assume a bandwidth of 20 MHz and 1 GHz for μ-wave and mm-wave, respectively. The LOS ball for the macro tier is assumed to be 200 m and the MBS density is assumed to be $\lambda_M = 1$ km^{-2}.

A. Simplifying Approximations and Validation of the Model

The last integral of (3) does not have a closed form. Consequently, we simplify the evaluation by expanding the exponential term in the numerator, i.e., $\exp(-2\lambda_S\sqrt{x^2 - r^2})$, with a power series, and evaluating each of the resulting integral terms separately. Furthermore, we use Newton–Cotes

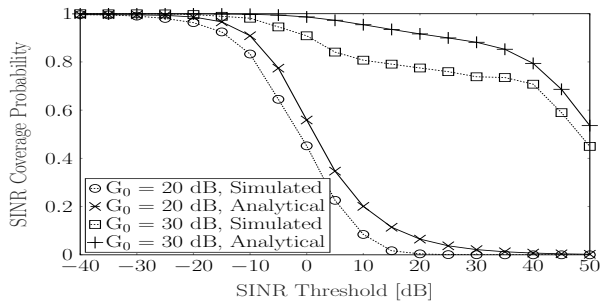

Figure 2: Validation of the analytical model for SINR coverage probability, $\lambda_S = 0.1$ m^{-1}, $\lambda_R = 1e-5$ m^{-2}.

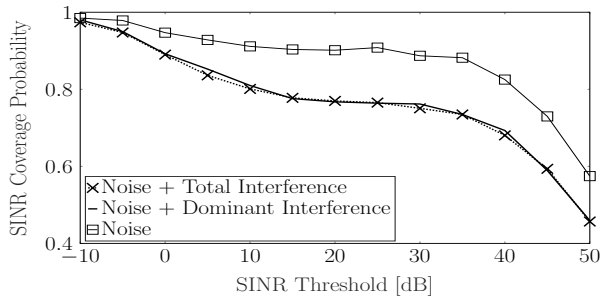

Figure 3: Validation of the mm-wave interference model, $\lambda_S = 0.1$ m^{-1}, $G_0 = 30$ dB.

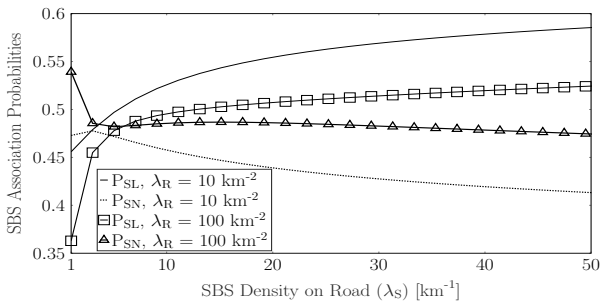

Figure 4: Association probabilities vs SBS density for different road density.

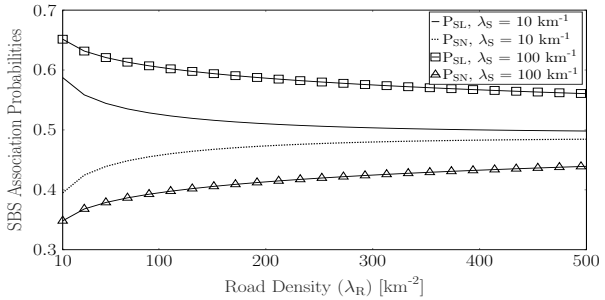

Figure 5: Association probabilities vs road density for different SBS density.

quadrature rule [14] to evaluate the outer integral of (4), as obtaining a closed form is not straightforward. To validate these approximations, in Fig. 2, we compare the SINR coverage probability obtained using our analytical framework with Monte Carlo simulations. We observe that the analytical results agree appreciably with the simulations. Specifically, we observe that the analytical results provide a tight upper bound to the simulations.

Furthermore, we also validate our assumption of the dominant interferer model to characterize the mm-wave interference (Section III A). In Fig. 3, we use Monte Carlo simulations to compare the actual SINR coverage probability of the typical user with that obtained by considering the interference only from dominant user, and the one considering a noise limited model. We see that the noise limited model is not a true representation of the actual SINR characteristics, whereas, the dominant interferer model quite accurately matches with the actual SINR coverage probability. Thus, the dominant interferer model can be used to represent the mm-wave interference.

B. Association and RAT Selection Probabilities

For the typical user, the perceived SBS density depends on both λ_R and λ_S. However, the effects of λ_R and λ_S are quite different. In Fig. 4 we plot $\mathbb{P}_{SL}$ and $\mathbb{P}_{SN}$. As λ_S increases for a given λ_R, the LOS SBS association probability increases. This is due to the fact that with increasing λ_S, the distance to the nearest SBS decreases. Although the number of NLOS SBSs also increases with increasing λ_S, their proximity to the typical user do not necessarily decrease significantly due to the fixed λ_R. On the contrary, with increasing λ_R, we observe that $\mathbb{P}_{SN}$ increases (see Fig. 5. This is due to the decreasing proximity of NLOS SBSs with increasing λ_R.

In Fig. 6 we plot the conditional mm-wave selection probability with respect to λ_S, given that the typical user has selected a LOS SBS. We observe that increasing G_0 has a more pronounced effect on the mm-wave RAT selection than increasing λ_S. For $G_0 = 26$ dB, $\lambda_S = 20$/km^2 ensures mm-wave service. Whereas, with 25 dB, the operator needs to have $\lambda_S = 100$/km^2 (5 fold increase). Thus, increasing the antenna gains in the transmitter and/or receiver is a more effective way of prioritizing mm-wave selection, than deploying more SBSs.

C. SINR Coverage Probabilities

In Fig. 7 we plot the SINR coverage probability for different λ_R and λ_S and two different values of G_0. Clearly, mm-wave (with $G_0 = 30$ dB) provides better SINR performance, precisely due to the large directional antenna gain and the fact that mm-wave transmissions suffer from minimal interference, i.e., only from the neighboring SBS. Furthermore, we observe that increasing λ_R (i.e., going from a sparser to denser urban scenario), or decreasing λ_S, decreases the SINR performance of the user. The decrease in coverage with increasing λ_R is because the interfering NLOS μ-wave signals increase. This highlights the fact that, although with increasing road density, the number of SBSs perceived by the typical user increases, it does not necessarily improve the SINR performance of the user. Therefore, in denser urban scenarios, the operator should necessarily deploy more SBS per road, to maintain the SINR performance of the user.

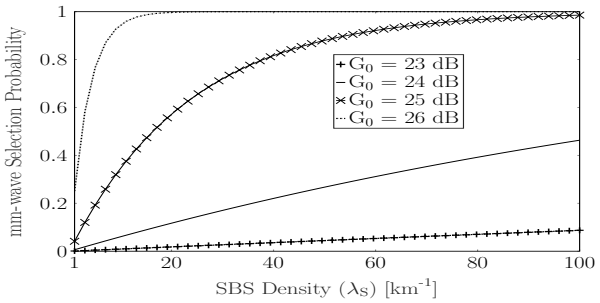

Figure 6: Conditional mm-wave selection probability.

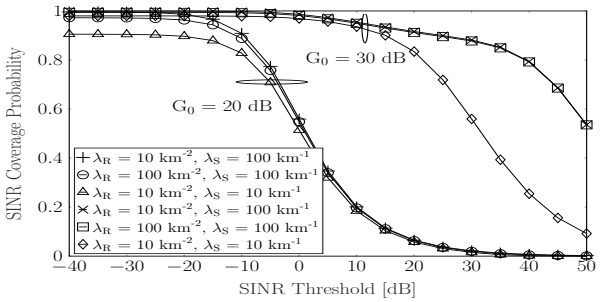

Figure 7: SINR coverage probability for various road and SBS densities.

On the other hand, decreasing λ_S increases the distance of the user from the nearest LOS SBS, thereby decreasing the useful signal power. This loss is more pronounced in the mm-wave association case with $G_0 = 30$ dB. This is due to the high path-loss of mm-wave signals, leading to severe deterioration in the useful signal power with decreasing λ_S.

Finally, we emphasize that the gain in SINR coverage by using higher antenna gains is dependent on λ_S. In Fig. 8, we plot the relative gain with $G_0 = 30$ dB with respect to $G_0 = 20$ dB, at $\gamma = -10$ dB. With $G_0 = 20$ dB, the typical user mostly selects μ-wave RAT, in contrast to mm-wave with $G_0 = 30$ dB. With λ_S, the gain initially increases, due to the decreasing proximity of the serving SBS. However, after a certain SBS density, the gain decreases due to increasing neighboring SBS interference. However, with very dense deployment we see that the gain saturates without decreasing further. Moreover, we see that with higher λ_R, the gain saturates at a higher value, as with higher λ_R, the μ-wave performance deteriorates due to increasing NLOS SBS interference. In fact, for very low λ_S (e.g., $\lambda_S \leq 10^{-4}$ m^{-1}), the gain may become negative, i.e., higher μ-wave RAT selection would provide better SINR performance. However, such sparse SBS deployments may not be realistic in urban heterogeneous networks. Thus, the SBS density to maximize the SINR performance can be optimized, which we will study in a future work.

VII. Conclusion

We have analytically characterized a multi-tier heterogeneous network, where small cells are deployed along the roads and employ both μ-wave and mm-wave RAT. We

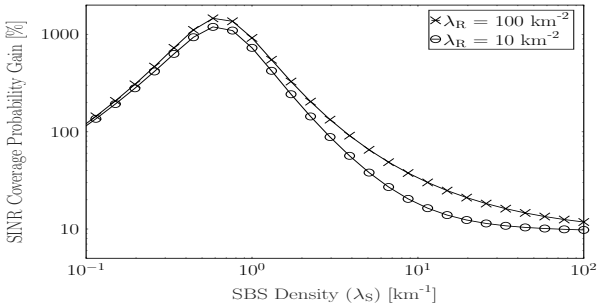

Figure 8: SINR coverage probability gain with mm-wave, γ = -10 dB.

observed that going from a sparse to a more dense urban scenario, with more roads in a given region, does not necessarily increase the SINR performance of the user, even by keeping the SBS density per street constant. Increasing the SBS deployment in a street efficiently improves the SINR coverage in μ-wave operation. However, for mm-wave operation, too large SBS deployment leads to a saturation in the gain in SINR performance. In a future work we will investigate optimizing the deployment parameters to guarantee coverage, while taking downlink data rate into account.

References

[1] T. S. Rappaport, *et al.*, "Millimeter Wave Mobile Communications for 5G Cellular: It Will Work!" *IEEE Access*, vol. 1, pp. 335–349, 2013.

[2] J. G. Andrews, F. Baccelli, and R. K. Ganti, "A tractable approach to coverage and rate in cellular networks," *IEEE Transactions on Communications*, vol. 59, no. 11, pp. 3122–3134, 2011.

[3] T. Bai and R. W. Heath, "Coverage and Rate Analysis for Millimeter-Wave Cellular Networks," *IEEE Trans. Wireless Commun.,*, vol. 14, no. 2, pp. 1100–1114, 2015.

[4] M. Di Renzo, "Stochastic Geometry Modeling and Analysis of Multi-Tier Millimeter Wave Cellular Networks," *IEEE Trans. Wireless Commun.*, vol. 14, no. 9, pp. 5038–5057, 2015.

[5] H. Elshaer, *et al.*, "Downlink and Uplink Cell Association With Traditional Macrocells and Millimeter Wave Small Cells," *IEEE Trans. Wireless Commun.*, vol. 15, no. 9, pp. 6244–6258, Sept. 2016.

[6] C.-H. Lee, C.-Y. Shih, and Y.-S. Chen, "Stochastic geometry based models for modeling cellular networks in urban areas," *Wireless networks*, vol. 19, no. 6, pp. 1063–1072, 2013.

[7] Y. J. Chun, M. O. Hasna, and A. Ghrayeb, "Modeling heterogeneous cellular networks interference using poisson cluster processes," *IEEE J. Sel. Areas Commun*, vol. 33, no. 10, pp. 2182–2195, 2015.

[8] F. Morlot, "A population model based on a Poisson line tessellation," in *2012 10th International Symposium on Modeling and Optimization in Mobile, Ad Hoc and Wireless Networks (WiOpt)*, May 2012, pp. 337–342.

[9] J. G. Andrews, *et al.*, "Modeling and analyzing millimeter wave cellular systems," *IEEE Transactions on Communications*, vol. 65, no. 1, pp. 403–430, Jan 2017.

[10] S. N. Chiu, *et al.*, *Stochastic geometry and its applications*. John Wiley & Sons, 2013.

[11] G. Ghatak, A. De Domenico, and M. Coupechoux, "Modeling and analysis of hetnets with mm-wave multi-rat small cells deployed along roads: Proofs," *arXiv preprint arxiv.org/abs/1704.02128*, 2017.

[12] H. Shokri-Ghadikolaei, *et al.*, "Millimeter Wave Cellular Networks: A MAC Layer Perspective," *IEEE Trans. Commun*, vol. 63, no. 10, pp. 3437–3458, 2015.

[13] H. Alzer, "On some inequalities for the incomplete gamma function," *Mathematics of Computation of the American Mathematical Society*, vol. 66, no. 218, pp. 771–778, 1997.

[14] M. Abramowitz and I. A. Stegun, *Handbook of mathematical functions: with formulas, graphs, and mathematical tables*. Courier Corporation, 1964, vol. 55.